Wideband Transmitarray Antenna Using Compact 2-Bit Filtering Unit Cells

Lehu Wen, Steven Gao, Qi Luo, Wei Hu, Benito Sanz-Izquierdo, Chao Wang, and Xue-xia Yang

Abstract—**A wideband transmitarray (TA) antenna using compact 2-bit filtering unit cells is presented with the center frequency designed at 10 GHz. The presented TA antenna features wide bandwidth with a compact aperture size, filtering radiation performance, and low cross-polarization levels. A novel compact 2-bit phasing scheme is first proposed and illustrated by utilizing the resonating characteristics of resonators. Charging and discharging principle of a resonator is utilized to realize a 180° phase shift, while J-invertor originating from the coupling between resonators is utilized to realize a 90° phase shift. Based on the proposed phasing scheme, novel 2-bit compact filtering unit cells are designed with a compact four-copper-layer configuration. Finally, a high-gain TA antenna was designed, fabricated, and measured for radiation performance verification. Owing to the elaborately designed unit cells and the cut-off effect of the feed horn, a filtering radiation performance with flat in-band gain and high out-of-band suppressions is obtained. Measured results show that a flat 3dB gain bandwidth of 21.3% is achieved with a thin thickness of $0.11\lambda_0$. High suppressions of 34.3 dB and 30.1 dB are measured over the lower and upper out-of-bands. In addition, a low cross-polarization level of -38.5 dB is obtained for high-quality wireless communications.**

Index Terms—**Filtering unit cell, resonator, transmitarray antenna, wideband array antenna.**

I. INTRODUCTION

High gain array antennas are especially desirable in long-distance wireless communication systems, such as satellites, radars, base stations, etc. Owing to the advantages of lightweight, low-profile, planar aperture, easy integration, and excellent electrical performances compared to conventional array antennas, transmitarray (TA) antennas are one of the most attractive antenna types for these systems. Benefiting from the unique spatial feed method, no additional feed networks are needed for the array elements. Therefore, low gain-loss with a simple and thin aperture can be achieved in TA antennas [1].

Different from the traditional array antennas using the feed networks for magnitude and phase distribution, TA antennas use unit cells to compensate the phase difference caused by the spatial feed. A classic method to realize full 360° spatial phase compensation is utilizing multi-layer frequency selective surface (FSS) structures [2]-[9]. Traditionally, stacked patches [2]-[3] and etched slots [4]-[5] can be utilized for realizing 360° phase delay. To reduce the thickness of the TA aperture, the element rotation method [6] and shorting vias [7]-[9] are utilized to realize the continuous 360° phase delay. By sequentially rotating the unit cell [6], a two-time phase delay can be

realized for circular polarization. Normally, the above methods are convenient to realize TA antennas with the foundations of FSS. However, due to the shared transmission and phase bandwidth by using the scaled FSS unit cells, the gain bandwidths of these developed TA antennas are normally limited for wideband wireless communications.

Another common method for TA antenna design is using receive-transmit antenna unit cells [10]-[18], where the bottom antenna receives the signal from the feed and the top antenna transmits the received signal to the free space. To reduce the design complexity and increase phase flexibility in receive-transmit unit cells, 1-bit phasing elements [12]-[14] are utilized to realize TA antennas. To increase the phase accuracy and aperture efficiency for TA antennas, 2-bit [15]-[16], 3-bit [17], and multiple discretized unit cells [18] are investigated. Recently, to efficiently suppress undesired interferences and increase the sensitivity of wireless communication systems, TA antennas with filtering radiation performance arouse great interest to researchers [19]-[21]. Normally, one can use a filtering antenna as the feed to illuminate an ordinary TA aperture [19] or the bandpass FSS elements [20] for a high-gain filtering radiation performance. In addition, unit cells can be designed with filtering characteristic.

In this work, a novel filtering TA antenna designed at 10 GHz is presented. A novel phasing scheme by using the resonating characteristics of resonators is proposed to design TA unit cells. In this scheme, charging and discharging principle of a resonator is utilized to realize a 180° phase shift, and resonator coupling working as a J-invertor is utilized to realize a 90° phase shift. Novel compact 2-bit filtering unit cells based on the line resonator and hair-pin resonator using the compact four copper layers are designed for TA antenna design. A new filtering TA antenna is then developed with flat in-band gain and high out-of-band suppressions. The filtering performance is benefiting from both the designed 2-bit unit cells and the cut-off effect of the designed feed horn. The presented filtering TA antenna was finally fabricated and measured for radiation performance verification. Measured results show that a wide 3dB gain bandwidth of 21.3% and low cross-polarization levels of -38.5 dB are achieved. High suppressions of 34.3 dB and 30.1 dB are obtained over the lower out-of-band the upper out-of-band.

II. 2-BIT UNIT CELLS

In this section, a new 2-bit phasing scheme is first proposed, which utilizes the different phasing characteristics of resonators for a stepped 90° delay. Novel compact four-layer receive-transmit unit cells are then developed for TA antenna design. The unit cells are simulated using the ideal periodic boundary in Ansys HFSS, and the relevant results are obtained under the normal incidence if there are no special specifications.

A. Phasing Scheme

Fig. 1 shows the proposed 2-bit phasing scheme. As shown in the figure, resonators are incorporated between the receiving and transmitting patches for different phase shifts. In this scheme, the tapping point of a resonator will be symmetrically changed to realize a 180° phase shift. In addition, the coupling between the cascaded

L. Wen is with the Department of Electronic and Electrical Engineering, University College London, WC1E 6BT, U.K. (LehuWen@ieee.org)

S. Gao is with the Department of Electronic Engineering, The Chinese University of Hong Kong, 999077, Hong Kong.

B. Sanz-Izquierdo and Chao Wang are with the School of Engineering and Digital Arts, University of Kent, Canterbury, CT2 7NT, U.K.

Q. Luo is with the School of Physics, Engineering and Computer Science, University of Hertfordshire, Hatfield, AL10 9AB, UK.

W. Hu is with the National Key Laboratory of Antennas and Microwave Technology, Xidian University, Xian, 710071, China.

X.-X. Yang is with the School of Communication and Information Engineering, Shanghai University, 200444, China.

resonators will be utilized to realize an additional 90° phase shift. Therefore, a discretized phase shift with a 90° phase step will be realized in the presented phasing scheme.
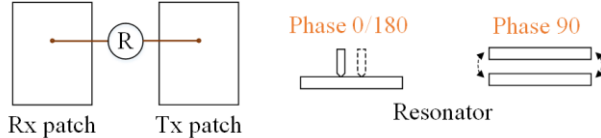

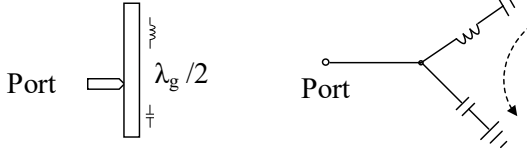Fig. 1. The proposed 2-bit phasing scheme.

Fig. 2. Equivalent circuit of a line-resonator for the realization of a 180° phase shift.

The 180° phase shift is realized by using the principle of charging and discharging to a resonator when the tapping position is symmetrically changed. Fig. 2 gives the equivalent circuit of a half-guided wavelength line-resonator with an offset tapping point for excitation. It can be seen that, the shorter section of the resonator below the tapping point can be seen as a capacitor, while the longer section above the tapping point can be seen as an inductor. Therefore, when the current enters into the line-resonator, it will first flow in the direction to the short section for charging the equivalent capacitor. After the half oscillation period, the current will return back to the long section for storing the energy in the equivalent inductor.

The 90° phase shift is realized by using the J-inverter introduced by the coupling between the resonators [22]. It is known that the coupling can be equivalent to an admittance inverter J [23]. The ABCD matrix of the J-inverter is

$$A_J = \begin{bmatrix} 0 & \pm\dfrac{1}{jJ} \\ \mp jJ & 0 \end{bmatrix} \qquad (1)$$

so the transmission coefficient for the admittance inverters is

$$S_{21}^J = \pm\frac{2j}{J + 1/J} \qquad (2)$$

Therefore, a 90° phase shift can be realized by using the coupling between resonators.

B. Phase 0°

Based on the proposed phasing scheme, a compact configuration of the TA unit cell 0 for phase 0° is developed and shown in Fig. 3. Two square patches with the lengths of L1 and L2 are designed on the bottom and top layers working as the receiving and transmitting patches. The second layer is the ground plane, which isolates the top and bottom patches. The third layer is the most important layer for the different phase states. For phase 0°, it is a half-wavelength line-resonator connected by two feedlines at each offset tapping point. A feedline is connected to the top transmit-patch through a buried via, while the other feedline is connected to the bottom receive–patch through another buried via. The periodic length of the unit cell is 14mm, which is $0.47\lambda_0$ (where λ_0 is the free space wavelength at 10 GHz). Two laminates of Rogers 4003C with the relative permittivity of 3.55 and thickness of 1.524 mm are used to print these four different copper layers. A bondply layer of Rogers 4450F with a thickness of 0.3 mm is used to bond these two laminates.

The connected line-resonator can be seen as a 1st-order bandpass filter. The initial tapping position can be obtained using the coupling parameter of Q_e=3.165 with the center working frequency at 10 GHz

[23]. The simulated S-parameters of this unit cell 0 are shown in Fig. 4, which is also compared to the S-parameters of the traditionally designed 2-bit reference unit cell 0 inset in this figure. Note that the reference unit cells in comparison have the same period length and the same thicknesses of the top and bottom laminates to ensure the same resonant quality of antennas.
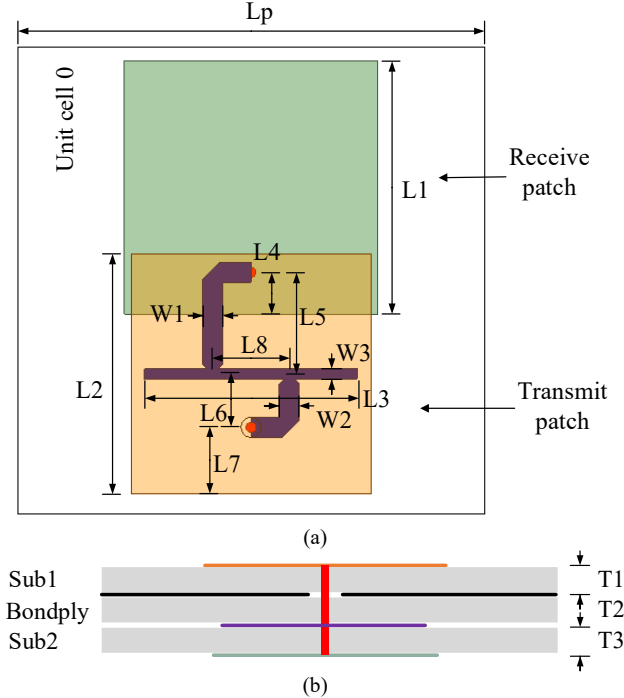

(a)

(b)

Fig. 3. Configuration of the unit cell for phase 0°. (a) Top view. (b) Side view. (Detailed parameters, Lp=14 mm, L1=7.6 mm, L2=7.2 mm, L3=6.4 mm, L4=1.2 mm, L5=3 mm, L6=1.6 mmm, L7=2 mm, L8=2.3 mm, W1=W2=0.6 mm, T1=T3=1.524 mm, T2=0.3 mm.)
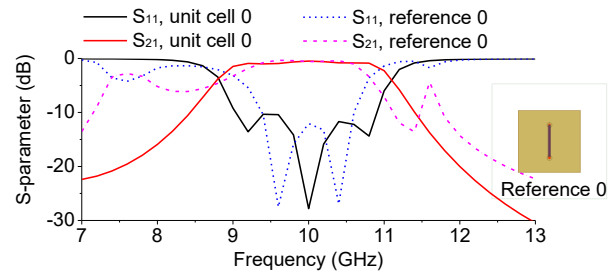

Fig. 4. S-parameters of the proposed unit cell 0 for phase 0°.

As shown in the figure, unit cell 0 has an obviously wide transmission bandwidth. In detail, the reflection coefficient of the proposed unit cell 0 has three zeroes, which are from the resonances of the top patch, the line-resonator, and the bottom patch. While the reference unit cell 0 only has two resonances as expected, and some undesired spurious resonances are also observed at both lower and upper out-of-band. In contrast, owing to the three resonances, wider bandwidth of 8.95-10.96 GHz is obtained for the transmission bandwidth of S_{21}>-2 dB. In addition, owing to the filtering effect of the line-resonator, undesired spurious resonances are successfully suppressed in both the lower and upper out-of-bands.

The designed unit cell 0 for the impinged wave under the different incident angles of 0° and 30° is investigated and the simulated results are shown in Fig. 5. First, Fig. 5(a) shows the S-parameters of the proposed unit cell 0. It can be seen that, when the incident angle changes from 0° to 30°, its -2 dB transmission bandwidth is almost unchanged with the reflection coefficient slightly increased. Whereas

the bandwidth of the reference 0 has a slight shift to the upper frequency with the in-band reflection coefficient also being deteriorated. In contrast, the proposed unit cell has a more stable transmission bandwidth. Fig. 5 (b) shows the transmission phase under the different incident angles. As can be seen, the phase of the presented unit cell 0 under the inclined 30° incidence is almost coincident with the phase under the normal incidence. At the two band-edges, there is a minor difference varying within ±5°. While the phase of reference 0 has a large phase difference of ±50° for the different incident angles within the interested bandwidth. Overall, stable transmission magnitude and phase can be obtained for the impinged wave under the different incident angles as compared to the referenced traditionally designed counterpart.
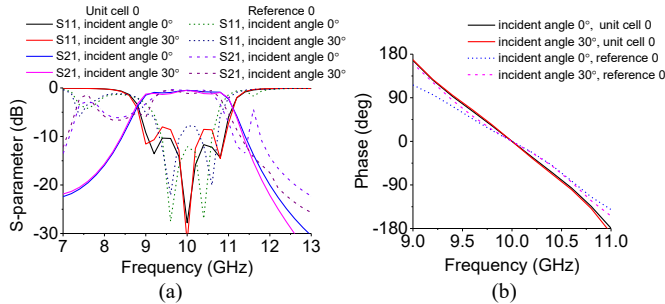

Fig. 5. (a) S-parameters and (b) transmission phase of the proposed unit cell 0 under different incident angles.
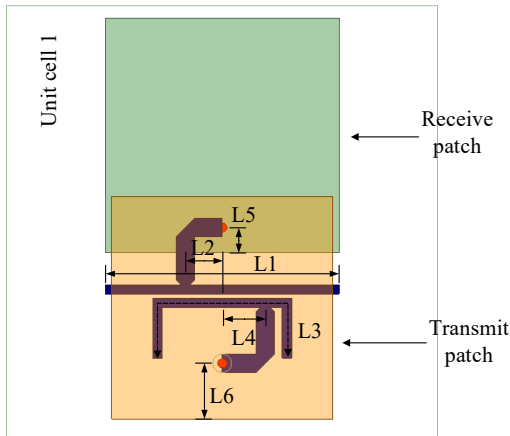

Fig. 6. Configuration of the unit cell 1 for phase shift -90°. (Detailed parameters, L1=7.6 mm, L2=1.2 mm, L3=7.8 mm, L4=1.4 mm, L5=0.8 mm, L6=1.8 mm. Note that the two ends of the line-resonator are open-circuited, and the visual difference on this resonator is due to the superposition of two colors.)
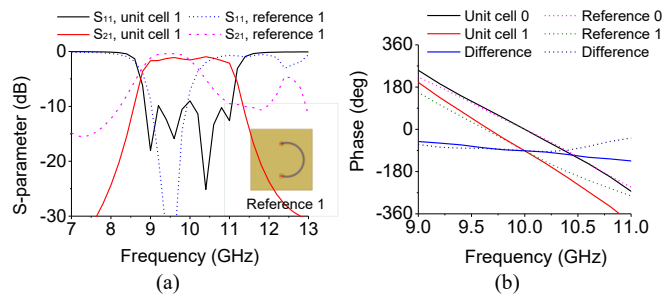

Fig. 7. (a) S-parameters and (b) phase response of the proposed unit cell 1 for phase shift -90°.

C. Phase -90°

The configuration of the TA unit cell 1 for phase -90° shift is shown in Fig. 6. It has very similar design parameters as the unit cell 0, except the parameters listed in the caption of the figure. Different

from unit cell 0, a half-wavelength hair-pin resonator is added on the third copper layer for a -90° phase shift. A 2nd-order coupling filter with the coupling parameters of Q_e=5.085 and M_{12}=0.257 [23] is referred to design this bandpass filter.

Fig. 7 (a) shows the simulated S-parameters of the designed unit cell 1 for a -90° phase shift. It can be seen that, owing to the introduction of the hair-pin resonator, there are four zeroes on the curve of the reflection coefficient. The transmission bandwidth for S_{21}>-2 dB is 8.95-10.95 GHz. The traditionally designed reference unit cell 1 is also designed and compared in this figure. Due to the distributed effect of the introduced phase delay line for -90° phase shift, a slight frequency shift to the lower frequency can be observed for the reference unit cell 1. Undesired spurious resonances still can be found at both lower and upper out-of-bands. Benefiting from the introduced line-resonator and hair-pin resonator, the proposed unit cell 1 has a good suppression over both the lower and upper out-of-bands, and a steep roll-off rate is observed at both lower and upper band-edges. The phase responses of the proposed unit cell 1 and 0 within bandwidth are shown in Fig. 7 (b), which are also compared to the traditionally designed reference 1 and 0. It can be seen that, a linear phase response is obtained for the presented unit cells, which leads to a linear phase difference. The phase variance of the presented unit cell is ±40° within the bandwidth, while the phase variance of the referenced unit cell is large than ±50°. The results in this figure show that a steep filtering response and a stable 90° phase delay are obtained by using the proposed resonator-based unit cells.
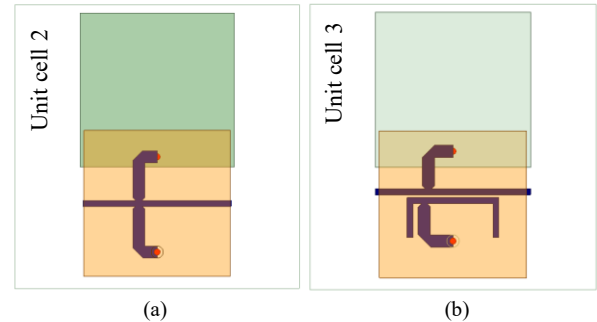
D. Phase -180° and -270°

Fig. 8. Configurations of the proposed (a) unit cell 2 and (b) unit cell 3 for delayed phase -180° and -270°. (Note that the two ends of the line-resonator in unit cell 3 are open-circuited, and the visual difference on this resonator is due to the superposition of two colors.)
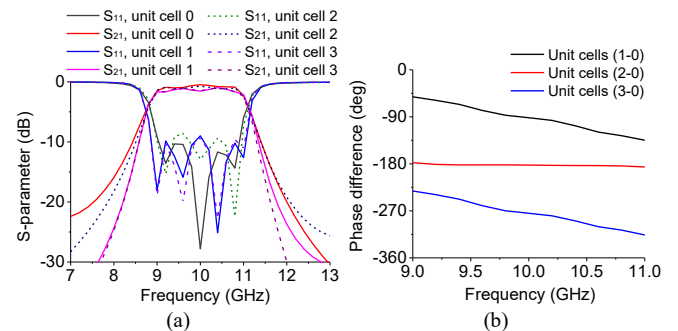

Fig. 9. (a) Magnitude and (b) phase response of the designed 2-bit unit cells.

By changing the tapping position on a resonator, as analyzed in Section II, an out-of-phase difference can be conveniently achieved for the other two unit cells. The configurations of unit cell 2 and unit cell 3 are shown in Fig. 8. Fig. 9 (a) gives the simulated S-parameters of the remaining 2-bit unit cells. As can be seen, after changing the tapping position, the S-parameters agree well with their

counterpart within the bandwidth. There is a slight difference in the out-of-band suppression due to weak cross-coupling caused by the resonator-feed difference. However, a very good accordance still can be achieved within the bandwidth and high suppression can be obtained at both lower and upper out-of-bands for the proposed 2-bit unit cells. The phase differences from unit cell 1, 2, and 3 to unit cell 0 are shown in Fig. 9 (b). It can be seen that the desired -90°, -180°, and -270° phase delays are obtained at the frequency of 10 GHz. Owing to the symmetrical change of the tapping point on the resonators, flat 180° phase delays are obtained between unit cells 0 and 2, and also between unit cells 1 and 3. For the phase difference between unit cells 0 and 1 and the difference between unit cells 2 and 3, the phase variances are small and less than ±40° within the whole bandwidth.

III. TRANSMITARRAY DESIGN

Based on the above-designed 2-bit filtering unit cells, a wideband TA antenna with 16×16 elements was developed, fabricated, and measured for radiation characteristic verification in this section.
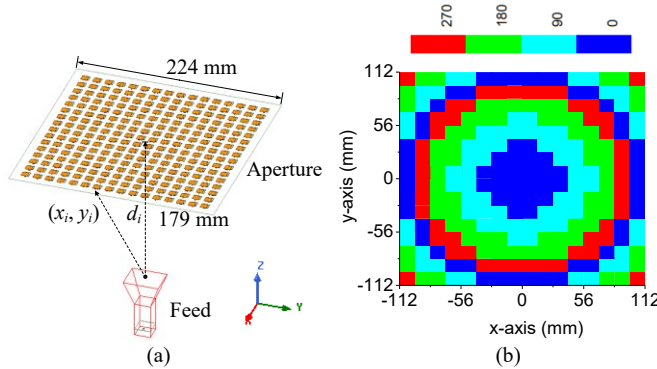

Fig. 10. (a) Configuration of the proposed CP RA antenna. (b) Required discretized phases of each unit cell.

A. Array Configuration

Fig. 10 (a) shows the configuration of the developed TA antenna. The TA aperture is in a square shape with a side length of 224 mm. A horn antenna working as the TA feed is 179 mm below the aperture center. The focal length to diameter ratio (f/D) is designed as 0.8 for this TA antenna. The horn antenna has a impedance bandwidth of 8.6-11.2 GHz with a peak realized gain of around 11 dBi and half-power beamwidth of around 48° in both two planes. Based on the TA configuration shown in this figure, the required phase distribution $\emptyset_R$ for each TA unit cell can be calculated using the equation below [1],

$$\emptyset_R = k_0(d_i - (x_i cos\varphi_b + y_i sin\varphi_b)sin\theta_b) \quad (3)$$

where k_0 is the propagation constant in vacuum, d_i is the distance of the phase center of the feed to the unit cell i, (x_i, y_i) is the coordinate of the unit cell i, and (θ_b, φ_b) is the array beam direction. According to (3), the required discretized 2-bit phase distribution at 10 GHz is obtained, discretized, and shown in Fig. 10 (b). The required phasing unit cells for the TA aperture are then selected according to the discretized phases in the figure.

B. Array Performance Investigation

The radiation characteristics of gain and aperture efficiency for the presented TA antenna are first investigated. By virtue of the resonators for different phase delays and the cut-off effect of the feed horn, the presented TA antenna has a unique feature of filtering radiation characteristic. Two cases of designs are compared to the presented TA antenna to illustrate this feature. The first is radiation performance obtained from the presented TA aperture fed by an ideal horn. The ideal horn is shown in Fig. 11 (a), which is a rectangular

waveguide with the same radiating aperture as the designed feed horn shown in Fig. 10 (a). It should be noted that the ideal horn is excited by using a wave port in simulation. Therefore, no mismatch loss will be existed for this ideal horn antenna. The second is the radiation performance obtained from the traditionally designed reference unit cells fed by the designed horn antenna. Note that all the 2-bit reference unit cells are shown in Fig. 11 (b), and they are designed with the configuration shown in Fig. 4 using the meander line for a 90° phase shift.
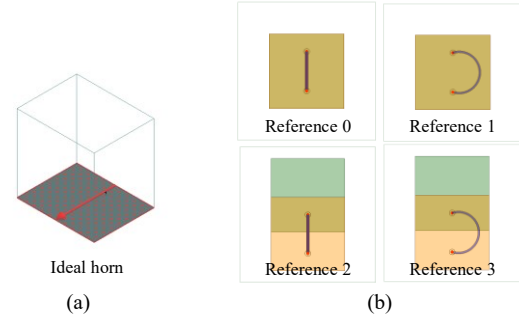

Fig. 11. (a) Ideal horn excited by using the wave port. (b) Traditionally designed unit cells for the reference TA antenna.
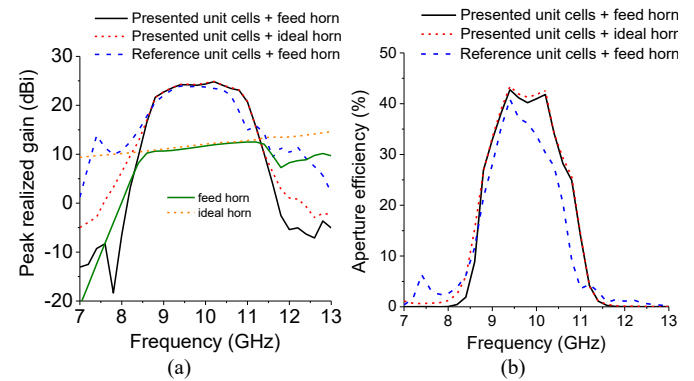

Fig. 12. (a) Simulated peak realized gain and (b) aperture efficiency of the presented TA antenna.

Fig. 12 gives the comparison results of these array antennas. The simulated peak realized gains of these antennas are first shown in Fig. 12 (a). It can be seen that the presented TA antenna fed by the elaborately designed horn antenna shows a good filtering characteristic. It has a flat in-band gain and high suppression over both lower and upper out-of-bands. In detail, its 3dB gain bandwidth covers 8.9-10.9 GHz. The suppression over the lower out-of-band of below 8 GHz is 33.1 dB, and the suppression over the upper out-of-band of beyond 12 GHz is 28.5 dB.

In contrast, when the presented TA aperture is fed by the ideal horn, it can be seen that a very similar in-band gain can be obtained. However, the filtering performance is worse than it is fed by the designed horn antenna. This is because the spill-over effect of the horn antenna will become significant when it works in the lower frequency band, while the ideal horn has a very linear gain over the whole frequency band owing to the ideal wave port excitation. In contrast, the designed horn antenna not only keeps the advantage of a linear gain in the interested band, but also has a reduced gain over lower and upper out-of-bands. Due to the cut-off effect of the waveguide, the designed horn antenna has more gain loss in the lower out-of-band than the gain in the upper out-of-band. The peak realized gain of the TA aperture designed using the reference unit cells (shown in Fig. 11 (b)) and fed by the designed horn antenna is also shown in this figure. It can be seen that, due to the narrow transmission bandwidth and no introduced filtering resonators, a narrow gain bandwidth is obtained with poor suppressions over both the lower and upper out-of-bands.

The AEs of these TA antennas are shown in Fig. 12 (b). It can be seen that the presented TA antenna has a peak AE of 42.8% at 9.4 GHz with the efficiency bandwidths of AE>40% from 9.3 GHz to 10.2 GHz and AE>30% from 8.9 GHz to 10.6 GHz. The presented TA aperture fed by the ideal horn has a slightly higher peak AE of 43.4% than it is fed by the designed horn antenna because of the perfect matching of the wave port in simulation. The reference TA antenna has the lowest AE due to the narrow bandwidth and the additional loss in the increased substrate layers for the phase delay line. Overall, owing to the introduced filtering 2-bit unit cells and the designed horn antenna, a filtering radiation performance with the flat in-band gain and high suppressions over both lower and upper out-of-bands is achieved for the presented TA antenna.

C. Results

The above-designed wideband TA antenna using the proposed 2-bit filtering unit cells was fabricated and measured at the University of Kent. Fig. 13 shows the photographs of the fabricated TA antenna prototype and the testing environment of its radiation performance in the anechoic chamber. Fig. 14 gives the measured peak realized gain and aperture efficiency of the fabricated prototype. The simulated results are also added in the figure for a good comparison.
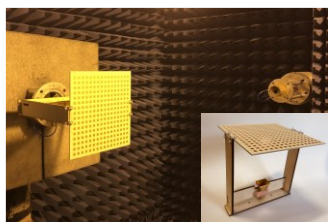

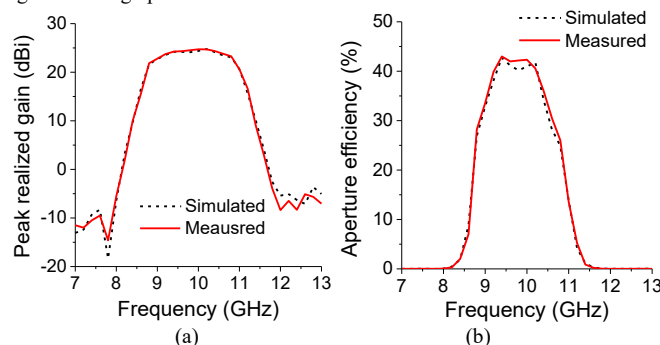Fig. 13. Photographs of the fabricated wideband TA antenna.

Fig. 14. Measured (a) peak realized gain and (b) aperture efficiency of the fabricated TA antenna.

As can be seen in Fig. 14 (a), a good filtering radiation characteristic is measured across the interested frequency band, as predicted by the simulated curve. A flat 3dB in-band gain covering 8.8-10.9 GHz is obtained with the maximum peak realized gain of 24.7 dBi. Steep roll-off rates can be observed at both lower and upper band-edges. In addition, high suppression of 34.3dB is measured over the lower out-of-band for the frequency less than 8GHz, and high suppression of 30.1dB is measured over the upper out-of-band for the frequency high than 12 GHz. The aperture efficiency is calculated from the measured peak realized gain, which is shown in Fig. 14 (b). It can be seen that the maximum AE is 42.9% within the bandwidth, and the bandwidth of AE>30% is from 8.85 GHz to 10.6 GHz.

The measured normalized E-plane and H-plane radiation patterns at 9 GHz, 10 GHz, and 10.8 GHz are shown in Fig. 15. As can be seen, there is a good agreement between the measured radiation patterns and the simulated results in both two planes. The measured half-power beamwidth varies from 7° to 8° in E-plane and also varies from 7° to 8° in H-plane. Low side-lobes are obtained with the side-lobe level 15.2 dB lower than the main beam across the entire

bandwidth. In addition, a very low cross-polarization level is measured, and its level is at least 38.5 dB lower than the main beam in the broadside direction. Overall, observing from the results shown in Fig. 14 and 15, a good consistency is achieved between the simulated and measured radiation performances. The slight differences between the measured and simulated results are mainly from the fabrication and assembly tolerances in the antenna prototype and position errors in the anechoic chamber.
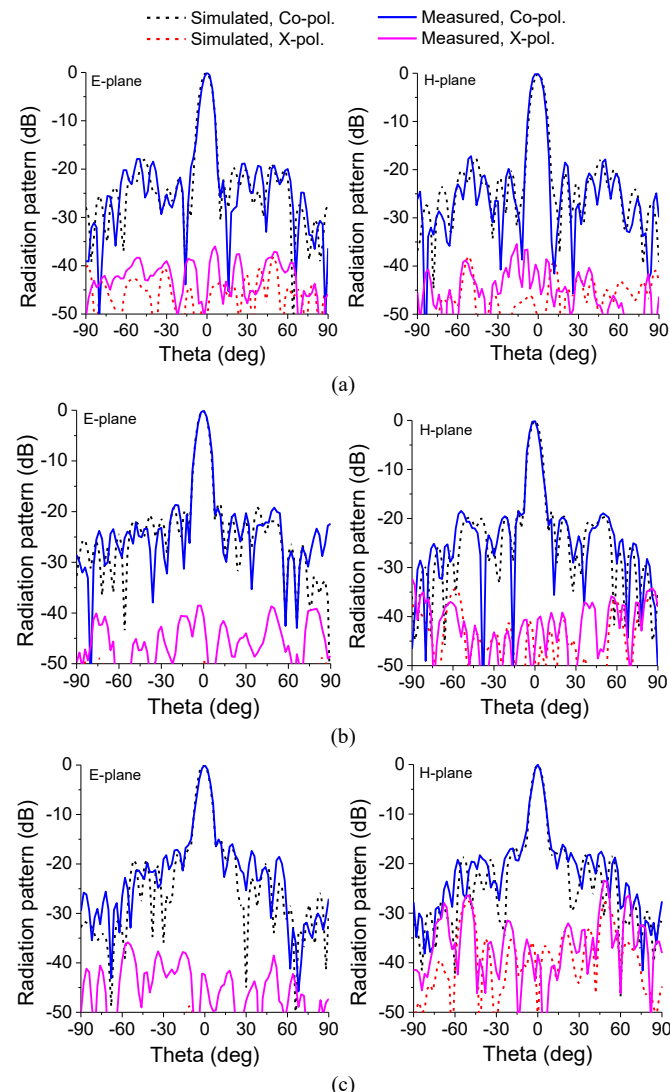

Fig. 15. Measured normalized radiation patterns of the fabricated TA antenna at (a) 9 GHz, (b) 10 GHz, and (c) 10.8 GHz.

D. Comparison

Table I compares the performances of the recently published TA antennas with our developed antenna, including the designs using the discretized 1-bit or 2-bit unit cells and the designs with the filtering radiation performance. In the table, λ_0 is the freespace wavelength at the center working frequency. It can be seen in [12]-[13] that, although 1-bit phasing scheme can efficiently reduce the design complexity for TA antennas, an undesired disadvantage is the relatively low AE due to the phase errors in unit cells. 2-bit unit cells in [15] can have an improve AE to 44.7%. Unfortunately, these TA antennas do not have the capability of spatial filtering function. To efficiently suppress undesired interference and reduce the burden of the active circuit systems for wireless communications, it is very meaningful to integrate the filtering performance into antennas. Traditionally, one can use multi-layer FSS to realize the spatial

TABLE I
COMPARISON OF THE RECENTLY PUBLISHED TA ANTENNAS

Reference	f_0 (GHz)	Gain BW	Aperture $\lambda_0 \times \lambda_0$	Thickness (λ_0)	PRG (dBi)	Peak AE	Phase	Suppression (dB)	XPD (dB)	Copper layers
[12]	13.5	13.1%	8.6×8.6	0.068	21.4	14.7%	1-bit	/	NG	3
[13]	27	40%	8.6×8.6	0.21	24.5	28%	1-bit	/	35	6
[15]	30	43.7%	8.9×8.9	0.21	26.1	44.7%	2-bit	/	35	5
[19]	60	10.3%	8×8	0.63	24.8	38%	FSS	L: 26.5 U: 28.8	22	6
[20]	30	16.9%	8.3×8.3	0.32	24.5	32%	FSS	L: 29.3 U: 33.3	33	9
[21]	35	7.3%	11.3×11.3	4.56	25.5	30%	5 UCs	L: 10.5 U: 33.5	35	2+lens
This work	10	21.3%	7.5×7.5	0.11	26.3	42.9%	2-bit	L: 34.3 U: 30.1	38.5	4

Abbreviations in the table, f_0: center frequency, BW: bandwidth, NG: not given, PRG: peak realized gain, UCs: unit cells, L: lower out-of-band, U: upper out-of-band, XPD: cross-polarization discrimination.

filtering function as the designs in [19]-[20]. However, this will incur large numbers of PCB layers and an increased fabrication cost. TA antenna in [21] uses five different 3D-printed lenses for discretized phase shifts, therefore a high profile of $4.56\lambda_0$ is achieved for the designed TA aperture. Compared to these designs, our presented wideband TA antenna not only owns a low profile of $0.11\lambda_0$ and a simple 4-layer PCB configuration, but also has high suppressions of 34.3 dB and 30.1 dB over both lower and upper out-of-bands and a high cross-polarization discrimination of 38.5 dB.

IV. CONCLUSION

A wideband TA antenna using compact 2-bit unit cells has been presented. A novel 2-bit phasing scheme is proposed and illustrated for 90° stepped phase shifts. Charging and discharging principle of a resonator is utilized to realize a 180° phase shift, and coupling between resonators is utilized to realize a 90° phase shift. Based on this scheme, novel 2-bit unit cells are designed and studied. A high-gain TA antenna with the center frequency designed at 10 GHz is then developed for the final radiation performance verification. By virtue of the filtering unit cells and the cut-off effect of the feed horn, a good filtering radiation performance is achieved. Detailed measured results show that the developed TA antenna can have a flat 3dB gain bandwidth of 21.3% and high out-of-band suppressions with a low aperture profile of $0.11\lambda_0$. These good results prove that the developed TA antenna can be a good candidate for anti-interference and high-quality wireless communications.

REFERENCES

[1] J. Huang and J. A. Encinar, *Reflectarray Antennas*. New York, NY, USA: IEEE Press, 2008.

[2] A. H. Abdelrahman, P. Nayeri, A. Z. Elsherbeni, and F. Yang, "Bandwidth improvement methods of transmitarray antennas," *IEEE Trans. Antennas Propag.*, vol. 63, no. 7, pp. 2946-2954, July 2015.

[3] B. Rahmati and H. R. Hassani, "Low-profile slot transmitarray antenna," *IEEE Trans. Antennas Propag.*, vol. 63, no. 1, pp. 174-181, Jan. 2015.

[4] R. Y. Wu, Y. B. Li, W. Wu, C. B. Shi, and T. J. Cui, "High-gain dual-band transmitarray," *IEEE Trans. Antennas Propag.*, vol. 65, no. 7, pp. 3481-3488, July 2017.

[5] S. L. Liu, X. Q. Lin, Z. Q. Yang, Y. J. Chen and J. W. Yu, "W-band low-profile transmitarray antenna using different types of FSS units," *IEEE Trans. Antennas Propag.*, vol. 66, no. 9, pp. 4613-4619, Sept. 2018.

[6] X. Zhang, F. Yang, S. Xu, A. Aziz and M. Li, "Dual-layer transmitarray antenna with high transmission efficiency," *IEEE Trans. Antennas Propag.*, vol. 68, no. 8, pp. 6003-6012, Aug. 2020.

[7] W. An, S. Xu, F. Yang and M. Li, "A double-layer transmitarray antenna using malta crosses with vias," *IEEE Trans. Antennas Propag.*, vol. 64, no. 3, pp. 1120-1125, March 2016.

[8] X. Yi, T. Su, X. Li, B. Wu and L. Yang, "A double-layer wideband transmitarray antenna using two degrees of freedom elements around 20 GHz," *IEEE Trans. Antennas Propag.*, vol. 67, no. 4, pp. 2798-2802, April 2019.

[9] W. Hu et al., "A wideband metal-only transmitarray with two-layer configuration," *IEEE Antennas Wireless Propag. Lett.*, vol. 20, no. 7, pp. 1347-1351, July 2021.

[10] Q. Luo et al., "A hybrid design method for thin-panel transmitarray antennas," *IEEE Trans. Antennas Propag.*, vol. 67, no. 10, pp. 6473-6483, Oct. 2019.

[11] Y.-M. Cai et al., "A novel ultrawideband transmitarray design using tightly coupled dipole elements," *IEEE Trans. Antennas Propag.*, vol. 67, no. 1, pp. 242-250, Jan. 2019.

[12] Y. Wang, S. Xu, F. Yang and M. Li, "A novel 1 bit wide-angle beam scanning reconfigurable transmitarray antenna using an equivalent magnetic dipole element," *IEEE Trans. Antennas Propag.*, vol. 68, no. 7, pp. 5691-5695, July 2020.

[13] F. Wu, J. Wang, R. Lu, X. Xia, W. Hong and K. -M. Luk, "Wideband and low cross-polarization transmitarray using 1 bit magnetoelectric dipole elements," *IEEE Trans. Antennas Propag.*, vol. 69, no. 5, pp. 2605-2614, May 2021.

[14] S. Liu, H. Sato and Q. Chen, "A wideband, 1 bit transmitarray antenna design with flat gain response," *IEEE Trans. Antennas Propag.*, vol. 68, no. 10, pp. 7046-7055, Oct. 2020.

[15] P. Mei, G. F. Pedersen and S. Zhang, "A broadband and FSS-based transmitarray antenna for 5G millimeter-wave applications," *IEEE Antennas Wireless Propag. Lett.*, vol. 20, no. 1, pp. 103-107, Jan. 2021.

[16] B. J. Xiang, X. Dai and K. -M. Luk, "A wideband 2-bit transmitarray antenna for millimeter-wave vehicular communication," *IEEE Trans. Veh. Technol.*, vol. 71, no. 9, pp. 9202-9211, Sept. 2022.

[17] K. T. Pham, A. Clemente, D. Blanco and R. Sauleau, "Dual-circularly polarized high-gain transmitarray antennas at Ka-band," *IEEE Trans. Antennas Propag.*, vol. 68, no. 10, pp. 7223-7227, Oct. 2020.

[18] K. Pham et al., "Design of wideband dual linearly polarized transmitarray antennas," *IEEE Trans. Antennas Propag.*, vol. 64, no. 5, pp. 2022-2026, May 2016.

[19] H. -T. Hu, G. -B. Wu, K. F. Chan and C. H. Chan, "V-band dual-polarized filtering transmitarray antenna enabled by a planar filtering illumination source," *IEEE Trans. Antennas and Propag.*, vol. 70, no. 10, pp. 9184-9197, Oct. 2022.

[20] P. -Y. Feng, S. -W. Qu, K. F. Chan, S. Yang and C. H. Chan, "Integrative transmitarray with gain-filtering and low-scattering characteristics," *IEEE Trans. Antennas Propag.*, vol. 70, no. 3, pp. 1931-1939, March 2022.

[21] P. Mei, S. Zhang, X. Q. Lin and G. F. Pedersen, "A millimeter-wave gain-filtering transmitarray antenna design using a hybrid lens," *IEEE Antennas Wireless Propag. Lett.*, vol. 18, no. 7, pp. 1362-1366, July 2019.

[22] C. -X. Mao, S. S. Gao, Y. Wang and J. T. Sri Sumantyo, "Compact broadband dual-sense circularly polarized microstrip antenna/array with enhanced isolation," *IEEE Trans. Antennas Propag.*, vol. 65, no. 12, pp. 7073-7082, Dec. 2017.

[23] J.-S. Hong and M. J. Lancaster, *Microstrip Filters for RF/Microwave Applications*. New York, NY, USA: Wiley, 2001.